The Astrophysical Journal Supplement Series, 254:26 (12pp), 2021 June https://doi.org/10.3847/1538-4365/abf656

Identifying the 3FHL Catalog. V. Results of the CTIO-COSMOS Optical Spectroscopy Campaign 2019

M. Rajagopal[1], S. Marchesi[1,2], A. Kaur[3], A. Domínguez[4], R. Silver[1], and M. Ajello[1]
[1] Department of Physics and Astronomy, Clemson University, Clemson, SC 29634, USA; changar@clemson.edu
[2] INAF—Osservatorio di Astrofisica e Scienza dello Spazio di Bologna, Via Piero Gobetti, 93/3, I-40129, Bologna, Italy
[3] Department of Astronomy and Astrophysics, 525 Davey Lab, Pennsylvania State University, University Park, PA 16802, USA
[4] IPARCOS and Department of EMFTEL, Universidad Complutense de Madrid, E-28040 Madrid, Spain
Received 2020 December 14; revised 2021 April 7; accepted 2021 April 7; published 2021 May 19

Abstract

As a follow-up to the optical spectroscopic campaign aimed at achieving completeness in the Third Catalog of Hard Fermi-LAT Sources (3FHL), we present here the results of a sample of 28 blazars of an uncertain type observed using the 4 m telescope at Cerro Tololo Inter-American Observatory in Chile. Out of these 28 sources, we find that 25 are BL Lacertae objects (BL Lacs) and 3 are flat-spectrum radio quasars (FSRQs). We measure redshifts or lower limits for 16 of these blazars, and it is observed that the 12 remaining blazars have featureless optical spectra. These results are part of a more extended optical spectroscopy follow-up campaign for 3FHL blazars, where, until now, 51 blazars of an uncertain type have been classified into BL Lac and FSRQ categories. Furthermore, this campaign has resulted in redshift measurements and lower limits for 15 of these sources. Our results contribute toward attaining a complete sample of blazars above 10 GeV, which then will be crucial in extending our knowledge on blazar emission mechanisms and the extragalactic background light.

Unified Astronomy Thesaurus concepts: Active galactic nuclei (16); Blazars (164); Active galaxies (17); Galaxy nuclei (609); Spectroscopy (1558); Interstellar emissions (840); Optical observatories (1170); Optical observation (1169)

Supporting material: data behind figure

1. Introduction

The Large Area Telescope (LAT; Atwood et al. 2009) on board the Fermi Gamma-Ray Space Telescope has enabled great strides in the understanding of blazars, the most powerful class of active galactic nuclei (AGN). Blazars make up the majority of the astrophysical gamma-ray source population (Abdollahi et al. 2020). The broadband spectral energy distribution (SED) of blazars is generally characterized by two distinct bumps, which are attributed to synchrotron radiation at lower energies (infrared to X-rays) and inverse Compton scattering at high energies (X-rays to gamma-rays, Maraschi et al. 1994; Abdo et al. 2011).

The Third Catalog of Hard Fermi-LAT Sources (3FHL; Ajello et al. 2017) reported 1556 sources detected in the 10 GeV–2 TeV energy range during the first seven years of Fermi-LAT's operation. Blazars represent the majority (∼1300/1556) of these 3FHL sources. However, ∼45% (578) of these blazars lack a redshift measurement and ∼21% (232) are of an uncertain type, leaving the 3FHL catalog highly incomplete.

Accurate redshift determinations are essential for studying numerous topics, including blazar emission processes and energetics (e.g., Ghisellini et al. 2017; van den Berg et al. 2019), the role of blazars in cosmic-ray acceleration (e.g., Furniss et al. 2013), the properties and evolution of extragalactic background light (EBL, i.e., the integrated emission from all stars and galaxies in the universe since the reionization epoch; e.g., Abramowski et al. 2012; Ackermann et al. 2012; Domínguez & Ajello 2015; Abdollahi et al. 2018; Desai et al. 2019), the derivation of cosmological parameters using gamma-rays (e.g., Domínguez et al. 2019), and studying and understanding the cosmic evolution of blazars (e.g., Ajello et al. 2014; Paliya et al. 2020).

To this end, spectroscopic campaigns of blazars have been effectively conducted with 4 m, 8 m, and 10 m class telescopes to investigate the nature of these sources as well as to provide accurate redshift measurements (e.g., Sbarufatti et al. 2005; Shaw et al. 2012; Massaro et al. 2014; Paggi et al. 2014; Landoni et al. 2015; Ricci et al. 2015; Álvarez Crespo et al. 2016a, 2016b; Paiano et al. 2017, 2019, 2020; Peña-Herazo et al. 2017, 2020; Marchesi et al. 2018; Desai et al. 2019). The successes of these campaigns prove that the listed classes of telescopes are capable of distinguishing the two blazar subclasses, namely, BL Lacertae objects (BL Lacs) and flat-spectrum radio quasars (FSRQs).

FSRQs show broad emission features in their optical spectra and have higher average luminosities than BL Lacs, thus allowing easy measurement of their redshifts, while BL Lac spectra exhibit weak or very narrow emission lines (equivalent width (EW) $\leqslant 5$ Å; Urry & Padovani 1995; Marcha et al. 1996).

Blazars are further subdivided into three categories based on the position of their synchrotron peak frequency, $\nu_{\rm pk}^{\rm sy}$. Sources with $\nu_{\rm pk}^{\rm sy} < 10^{14}$ Hz are classified as low-synchrotron peak blazars (LSP), sources with $10^{14} < \nu_{\rm pk}^{\rm sy} < 10^{15}$ Hz are known as intermediate-synchrotron peak blazars, and sources with $\nu_{\rm pk}^{\rm sy} > 10^{15}$ Hz are categorized as high-synchrotron peak blazars (HSP). In the Fermi catalogs, BCU is a term used for classification for associated counterparts that (a) show blazar-like multifrequency behavior or (b) are classified as blazars of an uncertain type in the Roma-BZCAT (Massaro et al. 2009). The 3FHL contains 232 BCUs, 28 of which were targeted in this work. Spectroscopic observations of such sources will enable us to classify these sources and potentially measure their redshifts.

In this campaign, 51 BCUs have so far been classified into BL Lacs and FSRQ categories using optical spectroscopy. Spectroscopic redshifts were also obtained for 15 of these sources (Marchesi et al. 2018; Desai et al. 2019). In addition, machine-learning algorithms have provided tentative classifications for an additional 51 sources (Kaur et al. 2019; Silver et al. 2020).

In this work, we report the results from spectroscopic observations of 3FHL BCUs performed using the Cerro Tololo Ohio State Multi-Object Spectrograph (COSMOS) mounted on the 4 m Blanco telescope located at the Cerro Tololo Inter-American Observatory (CTIO) facility. The organization of this paper is as follows: In Section 2, we report the criteria used for the sample selection. In Section 3, we describe the observation methodology and the data analysis approach. In Section 4, we summarize the results of this campaign, with additional consideration given to sources that exhibit spectral features, while in Section 5, we present our conclusions.

2. Sample Selection

In this work, we report the observations of 28 sources performed with CTIO in 2019, constituting the third part of this campaign.[5] These sources were selected from BCUs in the 3FHL catalog based on the following criteria:

1. Lack of a redshift.
2. Optical magnitude in the V band of $V \leqslant 21.5$.
3. Being bright in 10 GeV–2 TeV band: ($f_{3\mathrm{FHL}} > 10^{-12}$ erg s^{-1} cm^{-2}). This condition ensures that the completeness of the 3FHL catalog moves to lower fluxes as more optical observations are performed.
4. Being observable from Cerro Tololo ($-80^{\circ} <$ decl. $< 20^{\circ}$), above an altitude of 40° and during our scheduled observations from April to June.

Details of all sources analyzed here have been summarized in Table 1. Optical magnitudes have been obtained from the 3FHL catalog (where the authors used USNO[6] or SDSS[7] archival data).

3. Observations and Data Reduction

All the source spectra for this work were obtained using the COSMOS mounted on the 4 m Blanco telescope located at the CTIO facility in Chile. The instrument was configured with the red grism and 0.″9 slit, to cover a wavelength range of $\lambda = [5000-9000]$ Å, corresponding to a dispersion of ∼4 Å pixel^{-1} and a spectral resolution of $R \sim 2100$. Wavelength calibration was performed with a precision of 0.04 Å. The fluctuations were found to be both positive and negative indicating a nonbiased wavelength calibration process. The observations were performed over three nights in 2019 April and over four nights in 2019 June. However, due to poor weather conditions, data from six nights in total was used in our analysis. The observing dates for all sources along with the exposure times and V-band magnitudes have been reported in Table 1.

Spectra for each source were obtained in triplicate or more, with varying exposure times, and the individual observations were combined to reduce the effects of instrumental noise and cosmic-ray contamination. Data reduction was performed using the standard IRAF pipeline (Tody 1986) including bias subtraction and correction for bad pixels. Flat-field normalization was also performed in order to remove any wavelength-dependent variations present in the flat-field source (but not in the observed spectrum). The reliability of the emission and absorption lines was obtained by comparing the features in each individual exposure. Additionally, all spectra were visually inspected to remove any artificial features.

Wavelength calibration for each source was performed using the mercury–neon (Hg–Ne) lamp. A lamp spectrum was obtained after each observation of a source to account for the possible shifts in the pixel–λ calibration, due to changes in the telescope position throughout the night. The spectra were independently inspected for emission and absorption features typical of those observed in BL Lac and FSRQ spectra (e.g., see Stickel et al. 1991; Marcha et al. 1996; Bade et al. 1998; Shaw et al. 2013). The presence of only absorption features in a spectrum indicates either absorption by the intervening medium (along the line of sight) or by the host galaxy (e.g., Ca II, G-band, NaD, Mg I, Ca+Fe lines). This enables us to set a spectroscopic lower limit of the redshift. All spectra were flux calibrated using a spectrophotometric standard. The standards were observed twice each night: one at the beginning of the night and one at the end, under the same observing conditions as the rest of the analysis. Finally, each source spectrum was corrected for Galactic reddening, using the $E(B-V)$ value obtained from NASA/IPAC Infrared Science Archive online tool,[8] based on Schlafly & Finkbeiner (2011).

4. Results

Results obtained from the spectral analysis of the sources have been reported in Table 2 (along with source classifications). Here, we report to the highest precision for which there is agreement among different features. The corresponding spectra are shown in Figure 1. To make the features more apparent, normalized spectra of our sources are also shown, which were obtained by dividing the flux-calibrated spectrum by a power-law fit of the continuum. The signal-to-noise ratio (S/N) of the normalized spectra (reported in Table 2) were obtained by measuring the ratio in at least five different regions in the featureless part of each spectrum.

To identify the various emission and absorption features, all spectra were individually inspected. A feature was considered reliable if its presence was verified in all the individual exposures. Sources were classified as FSRQs if the emission lines in their spectra had EW > 5 Å, and as BL Lacs if emission lines were observed with EW < 5 Å.

In this work, 25 out of 28 sources have been classified as BL Lacs, with 3 sources being classified as FSRQs. Further, redshifts (z) have been provided for 6 sources and lower limits on z for 10 more. The remaining 12 sources exhibited featureless optical spectra.

Comments have been provided for all the sources. Certain source spectra were also observed to be particularly noisy, inhibiting us from identifying any features. Tentative classifications have been provided for such sources.

[5] These observations were awarded as part of the Fermi-GI cycle 10, accepted proposal 101287, PI: S. Marchesi.
[6] https://www.usno.navy.mil/USNO/astrometry/optical-IR-prod
[7] http://www.sdss3.org/
[8] https://irsa.ipac.caltech.edu/applications/DUST/

Table 1
List of Sources and their Properties Sorted in the Order of Increasing R.A. Values

3FHL Source Name	Counterpart	R.A. J2000 (hh:mm:ss)	Decl. J2000 (hh:mm:ss)	$E(B-V)$ (mag)	AB Mag	Obs. Date	Exposure (s)	Continuum Slope
(1)	(2)	(3)	(4)	(5)	(6)	(7)	(8)	(9)
J0001.9-4155	1RXS J000135.5-415519	00:01:33.05	−41:55:24.31	0.0114	18.43	2019 Jun 15	3700	−2.25
J0102.8-2001	PMN J0102-2001	01:02:50.96	−20:01:58.30	0.0128	18.20	2019 Jun 15	4350	−1.91
J0659.5-6743	SUMSS J065932-674346	06:59:32.20	−67:43:46.00	0.1053	20.21	2019 Apr 20	6000	−1.98
J0709.1-1525	PKS 0706-15	07:09:12.28	−15:27:00.30	0.5537	17.12	2019 Apr 21	3000	−3.12
J0737.5-8247	SUMSS J073706-824836	07:37:06.80	−82:48:37.00	0.1606	17.63	2019 Apr 21	3600	−1.27
J0953.3-7659	SUMSS J095303-765804	09:53:04.38	−76:58:02.20	0.4551	18.69	2019 Apr 19	5100	−1.85
J1042.2-4128	1RXS J104204.1-412936	10:42:04.09	−41:29:35.99	0.0774	18.36	2019 Jun 13	4000	−4.92
J1130.7-3137	NVSS J113046-313805	11:30:46.10	−31:38:08.00	0.0533	16.07	2019 Apr 20	1800	+1.59
J1225.4-3447	1RXS J122534.0-344737	12:25:34.00	−34:47:37.00	0.0549	18.36	2019 Jun 12	4100	−3.94
J1328.9-5607	PMN J1329-5608	13:29:01.14	−56:08:02.65	0.4101	16.78	2019 Apr 19	1800	−2.78
J1339.0-2359	PKS 1336-237	13:39:01.70	−24:01:14.00	0.0678	17.49	2019 Apr 20	3000	−2.89
J1353.8-3936	NVSS J135345-393711	13:53:45.16	−39:37:11.40	0.0571	19.30	2019 Apr 21	5400	−0.18
J1442.5-4621	SUMSS J144236-462302	14:42:36.40	−46:23:02.00	0.1271	16.40	2019 Apr 19	3600	−2.46
J1455.4-7559	SUMSS J145543-760054	14:55:43.23	−76:00:54.61	0.1213	18.40	2019 Jun 12	5200	−1.10
J1457.8-4642	PMN J1457-4642	14:57:41.80	−46:42:10.00	0.1990	16.63	2019 Apr 20	1800	+0.41
J1514.7-0949	PMN J1514-0948	15:14:49.60	−09:48:38.00	0.0917	19.48	2019 Jun 13	4800	−1.28
J1542.1-2915	NVSS J154203-291509	15:42:03.10	−29:15:09.00	0.1553	18.72	2019 Jun 12	4900	−2.27
J1549.7-3045	NVSS J154946-304501	15:49:46.60	−30:45:01.00	0.1026	19.25	2019 Jun 13	5400	−1.60
J1604.6-4441	PMN J1604-4441	16:04:31.02	−44:41:31.97	0.7779	20.00	2019 Jun 15	6200	−0.92
J1647.3-6438	PMN J1647-6437	16:47:37.74	−64:38:00.26	0.1522	18.15	2019 Apr 20	3700	−0.62
J1849.2-1647	1RXS J184919.7-164726	18:49:19.70	−16:47:26.00	0.2714	18.43	2019 Jun 13	2600	−1.84
J1934.2-2419	NVSS J193412-241922	19:34:12.69	−24:19:19.92	0.0939	17.26	2019 Jun 15	3400	−1.58
J1944.4-4523	1RXS J194422.6-452326	19:44:22.39	−45:23:30.12	0.0450	15.62	2019 Jun 13	900	−1.57
J1944.9-2143	1RXS J194455.3-214318	19:44:55.10	−21:43:18.84	0.0733	18.06	2019 Jun 12	3900	−2.48
J1955.0-5640	1RXS J195503.1-564031	19:55:03.00	−56:40:31.08	0.0453	17.25	2019 Jun 12	3100	−1.98
J2002.5-7119	1RXS J200234.9-711943	20:02:27.12	−71:19:40.80	0.0607	19.68	2019 Jun 12	3300	−1.81
J2058.8-1442	TXS 2056-149	20:58:46.74	−14:43:05.00	0.0351	15.38	2019 Jun 13	900	−0.75
J2309.7-3633	1RXS J230940.6-363241	23:09:40.85	−36 32 49.00	0.2731	17.75	2019 Jun 12	3150	−3.44

Note. The columns are: (1) 3FHL catalog (Ajello et al. 2017) name for the source, (2) optical, IR, X-ray, or radio counterpart of the source, (3) R.A., (4) decl., (5) $E(B-V)$ value obtained using the measurements of Schlafly & Finkbeiner (2011) and the NASA/IPAC Infrared Science Archive online tool, (6) V-band magnitude (AB system), (7) date of observation, (8) exposure time (in seconds) of the source under consideration, and (9) slope of the continuum fit obtained from the observed spectra.

4.1. Notes on Individual Sources

1. *3FHL J0001.9−4155*. The source optical spectrum showed one emission feature at 5450 Å (EW = 88 Å), resembling those observed in FSRQ spectra. However, the presence of only one such feature prevents us from successfully identifying it; thus, we tentatively classify it as an FSRQ. This source has been reported as an HSP blazar in the fourth catalog of AGN detected by the Fermi-LAT (4LAC; Ajello et al. 2020).
2. *3FHL J0102.8−2001*. The optical spectrum for this source showed an emission feature at 5107 Å (EW = 18 Å) and an absorption feature at 8084 Å. These features have been attributed to O II and NaD, respectively. This gives us an estimate of $z = 0.37$ for the source. This result is in mild disagreement with the previously reported value by Arsioli et al. (2015) in the 1WHSP catalog, which found a lower limit of $z > 0.38$ for this source. This lower limit on z was obtained by the authors assuming the host to be a standard candle (elliptical galaxy with $M_R = -22.9$). The nondetection of the host allows the authors to set a redshift lower limit for the source. This source has been reported as an HSP blazar in 4LAC.
3. *3FHL J0659.5−6743*. The optical spectrum for this source exhibited no features. This source has been classified as an HSP blazar in 4LAC.
4. *3FHL J0709.1−1525*. The optical spectrum for this source exhibits two absorption features at 5551 Å (Hβ) and 6017 Å (Ca+Fe), respectively. This result gives us $z > 0.142$ for this source which we classify as a BL Lac. This result is in mild disagreement with the redshift obtained by Paiano et al. (2020) of $z = 0.142$. Apart from the absorption features, the authors also found an emission feature at 7518 Å that they attributed to N II (6584 Å). This feature was not observed in our spectra for this source. Paiano et al. (2020) obtained the optical spectra for this source with the OSIRIS spectrograph at the 10.4 m GTC at Roque de Los Muchachos telescope facility. This source is an HSP blazar in 4LAC.
5. *3FHL J0737.5−8247*. The optical spectrum for this source displayed no features. This source has no reported SED class in the Fermi-LAT catalogs.
6. *3FHL J0953.3−7659*. The optical spectrum for this source showed no features and has been classified as an HSP blazar in 4LAC.
7. *3FHL J1042.2−4128*. In the optical spectrum for this source, the features identified were a G-band absorption

Table 2
Results Obtained from Spectral Analysis Discussed in Section 4

3FHL Source Name	S/N	Spectral Line Rest-frame λ (Å)	Observed λ (Å)	Line Type	Equivalent Width (Å)	Redshift	Classification
J0001.9-4155	25.36	⋯	5450	Emission	88	⋯	FSRQ*
J0102.8-2001	18.40	O II (3727)	5107	Emission	18	0.37	FSRQ*
		NaD (5892)	8084	Absorption			
J0659.5-6743	15.97						BL Lac
J0709.1-1525	39.40	Hβ (4861)	5551	Absorption		>0.14	BL Lac
		Ca+Fe (5269)	6017	Absorption			
J0737.5-8247	30.37						BL Lac
J0953.3-7659	13.94						BL Lac
J1042.2-4128	24.07	*G*-band (4304)	5210	Absorption		>0.21	BL Lac
		Mg I (5175)	6274	Absorption			
J1130.7-3137	39.41	Hβ (4861)	5609	Emission	2.4	0.15	BL Lac
		O III (5007)	5770	Emission	1.1		
J1225.4-3447	29.84	*G*-band (4304)	5994	Absorption		>0.39	BL Lac
		Ca+Fe (5269)	7336	Absorption			
J1328.9-5607	20.21	*G*-band (4304)	5063	Absorption		>0.17	BL Lac
		Mg I (5175)	6099	Absorption			
J1339.0-2359	23.29	O II (3727)	6165	Emission	47	0.65	FSRQ
		O III (5007)	8287	Emission	22		
J1353.8-3936	29.88	*G*-band (4304)	6440	Absorption		>0.49	BL Lac
		Ca+Fe (5269)	7875	Absorption			
J1442.5-4621	64.63	O III (5007)	5517	Emission	1.5	0.10	BL Lac
		Mg I (5175)	5698	Absorption			
		Ca+Fe (5269)	5806	Absorption			
		NaD (5892)	6492	Absorption			
J1455.4-7559	13.52						BL Lac
J1457.8-4642	36.07	Hβ (4861)	5372	Emission	0.6	0.10	BL Lac
		Mg I (5175)	5744	Absorption			
		Ca+Fe (5269)	5851	Absorption			
J1514.7-0949	21.56						BL Lac
J1542.1-2915	20.22						BL Lac
J1549.7-3045	12.38						BL Lac
J1604.6-4441	06.39						BL Lac
J1647.3-6438	43.31	Ca II (3934)	7195	Absorption		>0.82	BL Lac
		Ca II (3969)	7230	Absorption			
J1849.2-1647	68.07	Mg I (5175)	8537	Absorption		>0.64	BL Lac
		Ca+Fe (5269)	8659	Absorption			
		OR					
		Mg I (5175)	8659	Absorption		>0.67	
		Ca+Fe (5269)	8805	Absorption			
J1934.2-2419	26.89						BL Lac
J1944.4-4523	34.53	*G*-band (4304)	7274	Absorption		>0.68	BL Lac
		Mg I (5175)	8704	Absorption			
		Ca+Fe (5269)	8916	Absorption			
J1944.9-2143	20.29	Mg I (5175)	7289	Absorption		>0.41	BL Lac
		Ca+Fe (5269)	7435	Absorption			
J1955.0-5640	25.47	*G*-band (4304)	5255	Absorption		>0.22	BL Lac
		NaD (5892)	7198	Absorption			
J2002.5-7119	23.10						BL Lac
J2058.8-1442	35.05	O III (5007)	5375	Emission	0.4	0.07	BL Lac
		Mg I (5175)	5574	Absorption			
J2309.7-3633	43.26						BL Lac

Note. Classifications and redshift measurements marked with * are tentative results.

feature at 5210 Å and a Mg I feature at 6274 Å, respectively. These two features allowed us to establish a lower-limit redshift of $z > 0.21$ for this source. A featureless optical spectrum for this source was obtained by de Menezes et al. (2020) using the 4.1 m Southern Astrophysical Research Telescope (SOAR) at Cerro Pachón, Chile. We classify this source as a BL Lac. This source has been reported as an HSP blazar in 4LAC.

8. *3FHL J1130.7−3137*. The optical spectrum of this source displayed two emission features at 5609 Å and 5770 Å, corresponding to Hβ (EW = 2.4 Å) and O III (EW = 1.1 Å), respectively. This yields a redshift of $z = 0.15$ for the source. The 6dF Galaxy Survey (Jones et al. 2009)

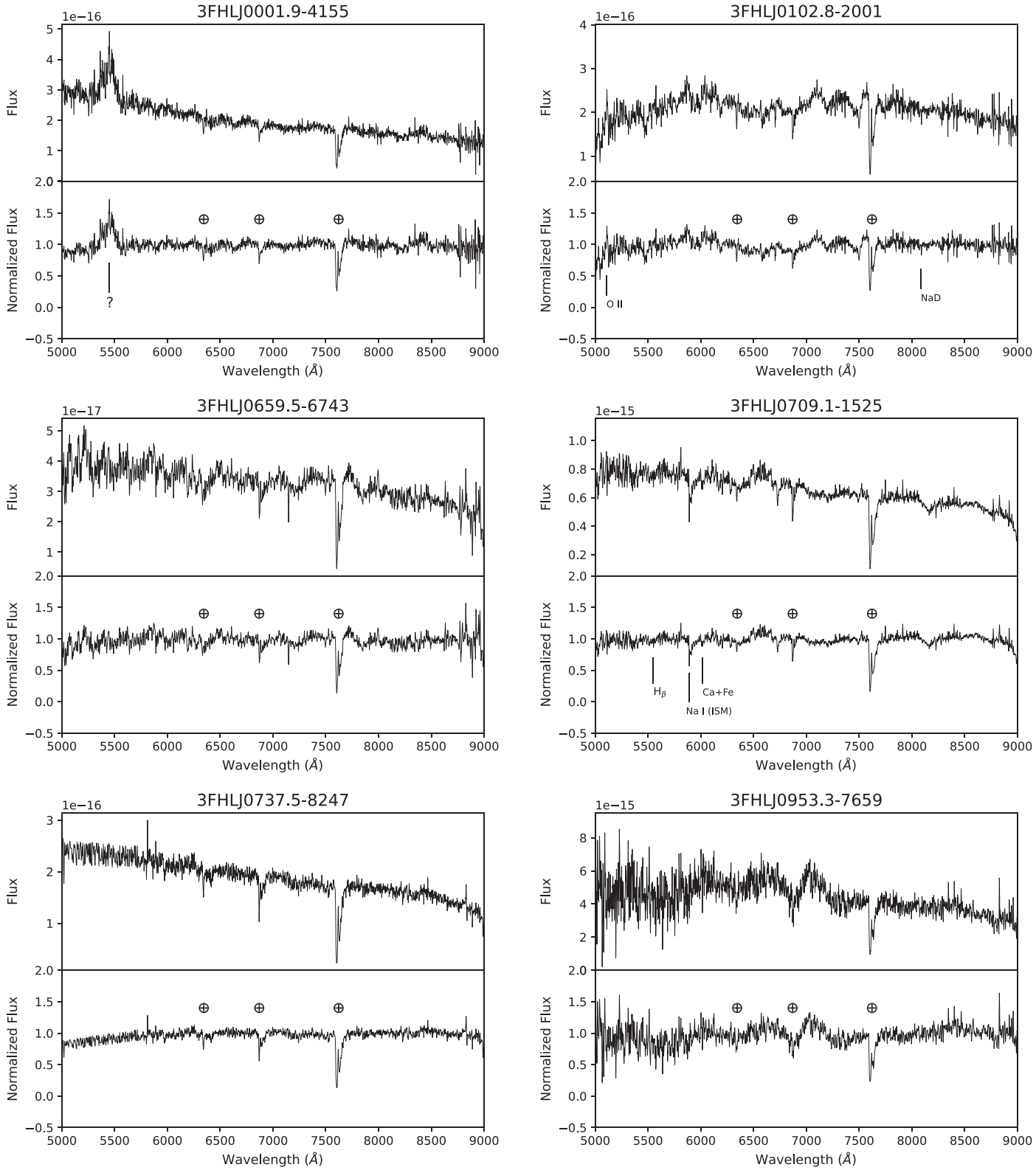

Figure 1. Normalized optical spectra of the observed candidates after performing flux calibration and dereddening. The atmospheric features are denoted by ⊕ while the absorption or emission features are labeled as per the lines they signify. The flux is in the units of erg cm^{-2} s^{-1} $Å^{-1}$.
(The data used to create this figure are available.)

obtained a spectrum for this source (obtained by the 6dF fiber-fed multiobject spectrograph at the United Kingdom Schmidt Telescope) from which they derived a redshift of 0.15, and classified the source as a BL Lac, in agreement with our results. This source has been classified as an HSP blazar in 4LAC.

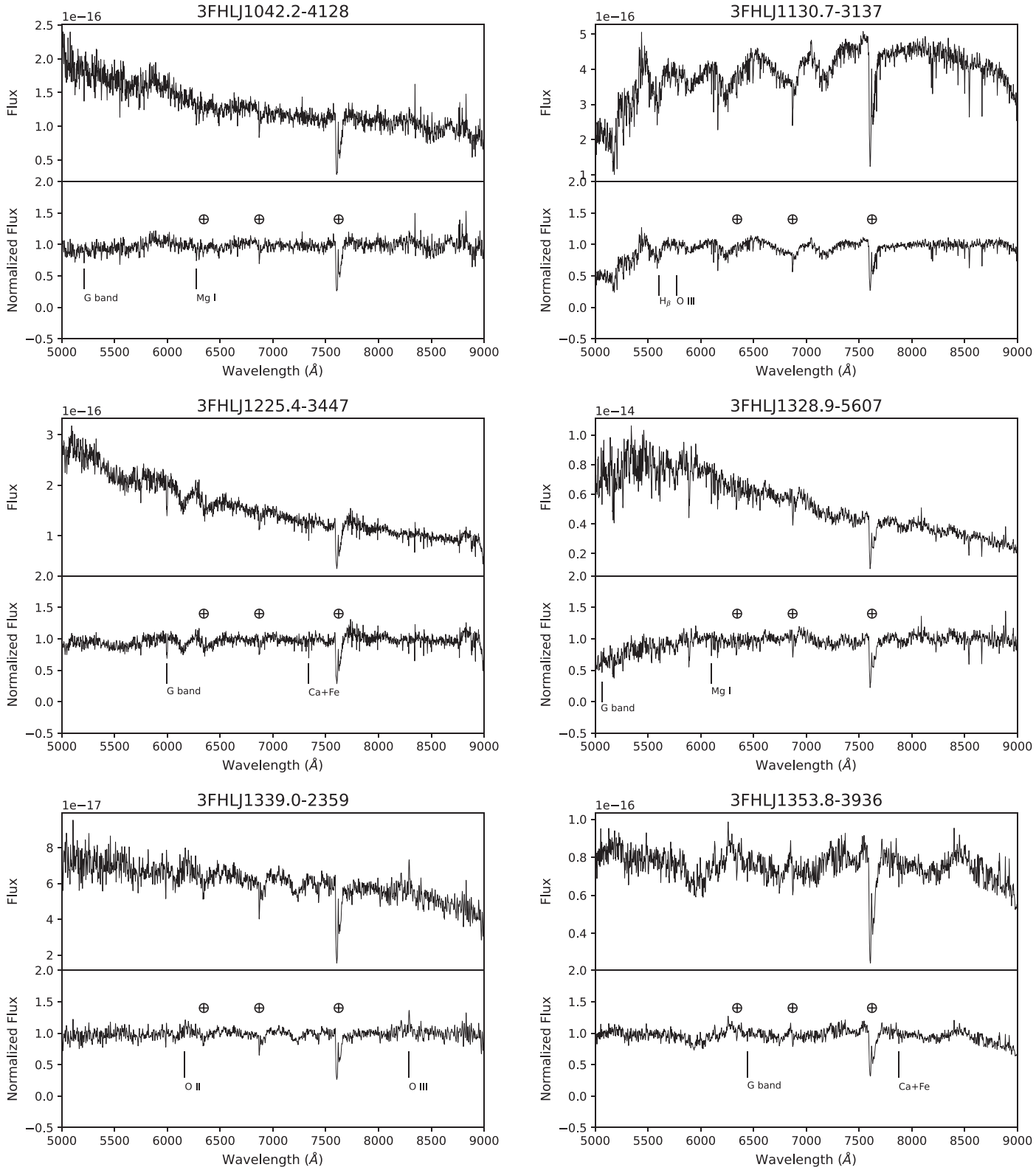

Figure 1. (Continued.)

9. *3FHL J1225.4−3447*. In the optical spectrum for this source, two absorption features were detected at 5994 Å, corresponding to the *G*-band, and 7336 Å, corresponding to Ca+Fe lines, respectively. This produces a redshift of $z > 0.39$ for the source, which we classify as a BL Lac. This source has been reported as an HSP blazar in 4LAC.

10. *3FHL J1328.9−5607*. The optical spectrum obtained for this source was noisy, but we were able to identify two absorption features at 5063 Å and 6099 Å, ascribed to *G*-band and Mg I lines, respectively. This yields a lower limit of $z > 0.17$ for this source. Our proposed lower-limit value is compatible with the value reported by Shaw et al. (2013)

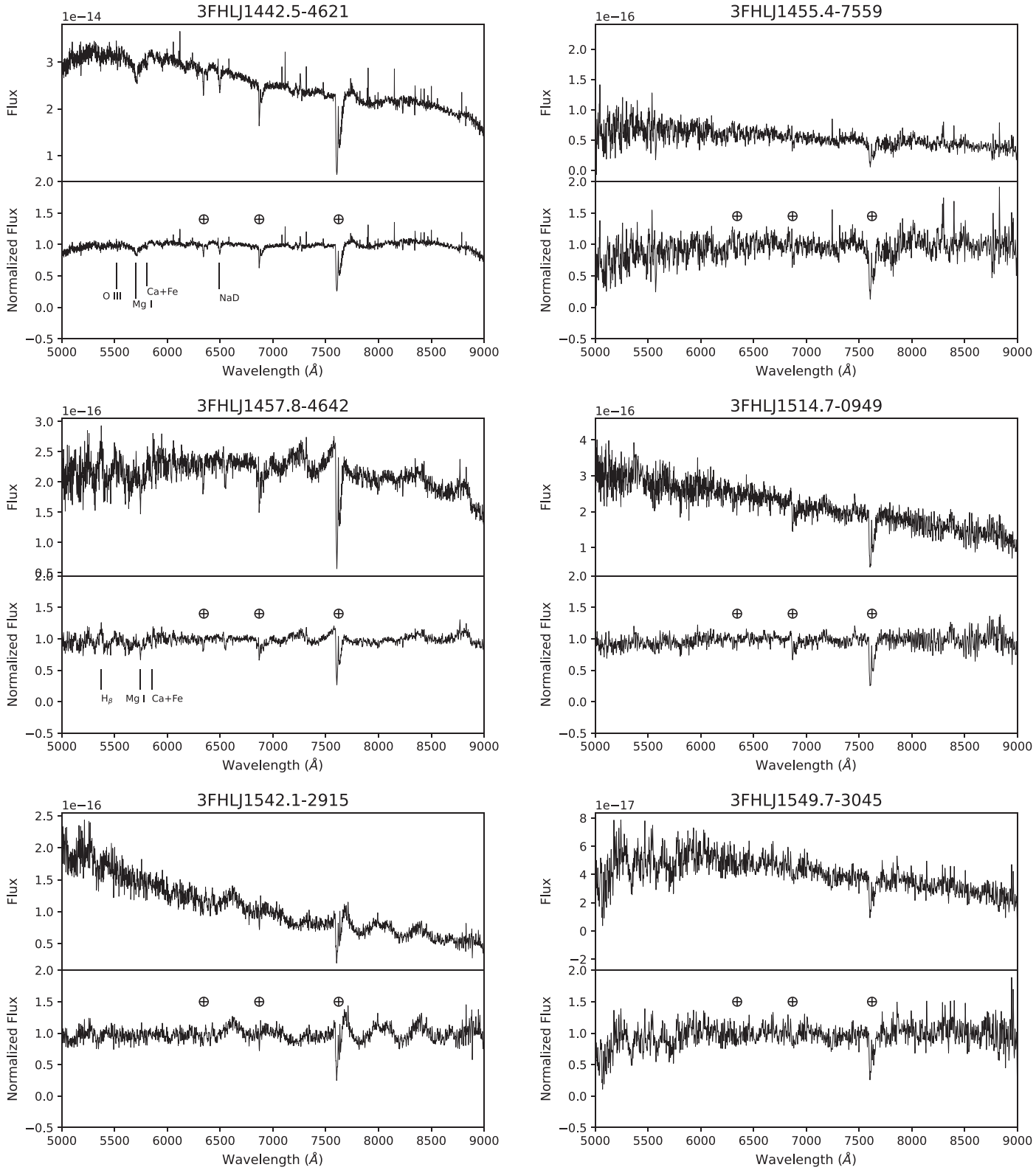

Figure 1. (Continued.)

of $z > 0.13$. This lower limit on z was obtained by the authors assuming the host to be a standard candle (elliptical galaxy with $M_R = -22.5$). While the authors were unable to determine whether the source is a BL Lac or an FSRQ, they reported it as an LSP blazar, in agreement with 4LAC. We classify this source as a BL Lac.

11. *3FHL J1339.0−2359*. This source has been reported as a BL Lac in the 4FGL catalog with a z of 0.657. Possible emission features at 6165 Å (O II, EW = 47 Å) and 8287 Å (O III, EW = 22 Å) agree with the measured redshift of $z = 0.65$. We classify this source as an FSRQ. The redshift for this source was first measured

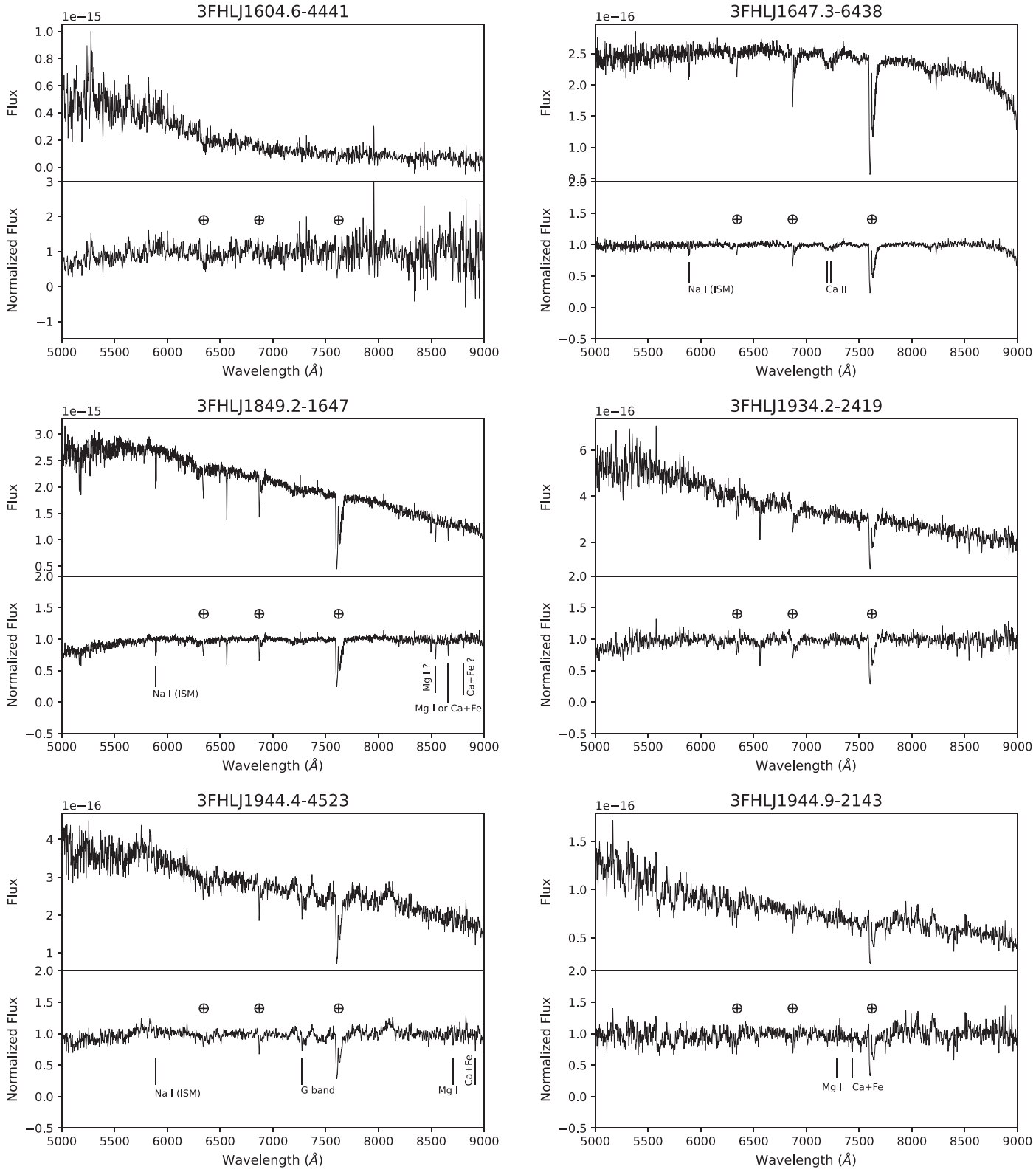

Figure 1. (Continued.)

by Malkin (2016), in the Optical Characteristic of Astrometric Radio Sources catalog, which was then referred to by the very long baseline interferometry catalog by Truebenbach & Darling (2017). This source has been reported as an LSP blazar in 4LAC.

12. *3FHL J1353.8−3936*. Our fairly noisy optical spectrum for this source allowed us to find two absorption features at 6440 Å (*G*-band) and 7875 Å (Ca+Fe), respectively, yielding a redshift of $z > 0.49$. We classify this source as a BL Lac. This source has been reported as an HSP blazar in 4LAC.

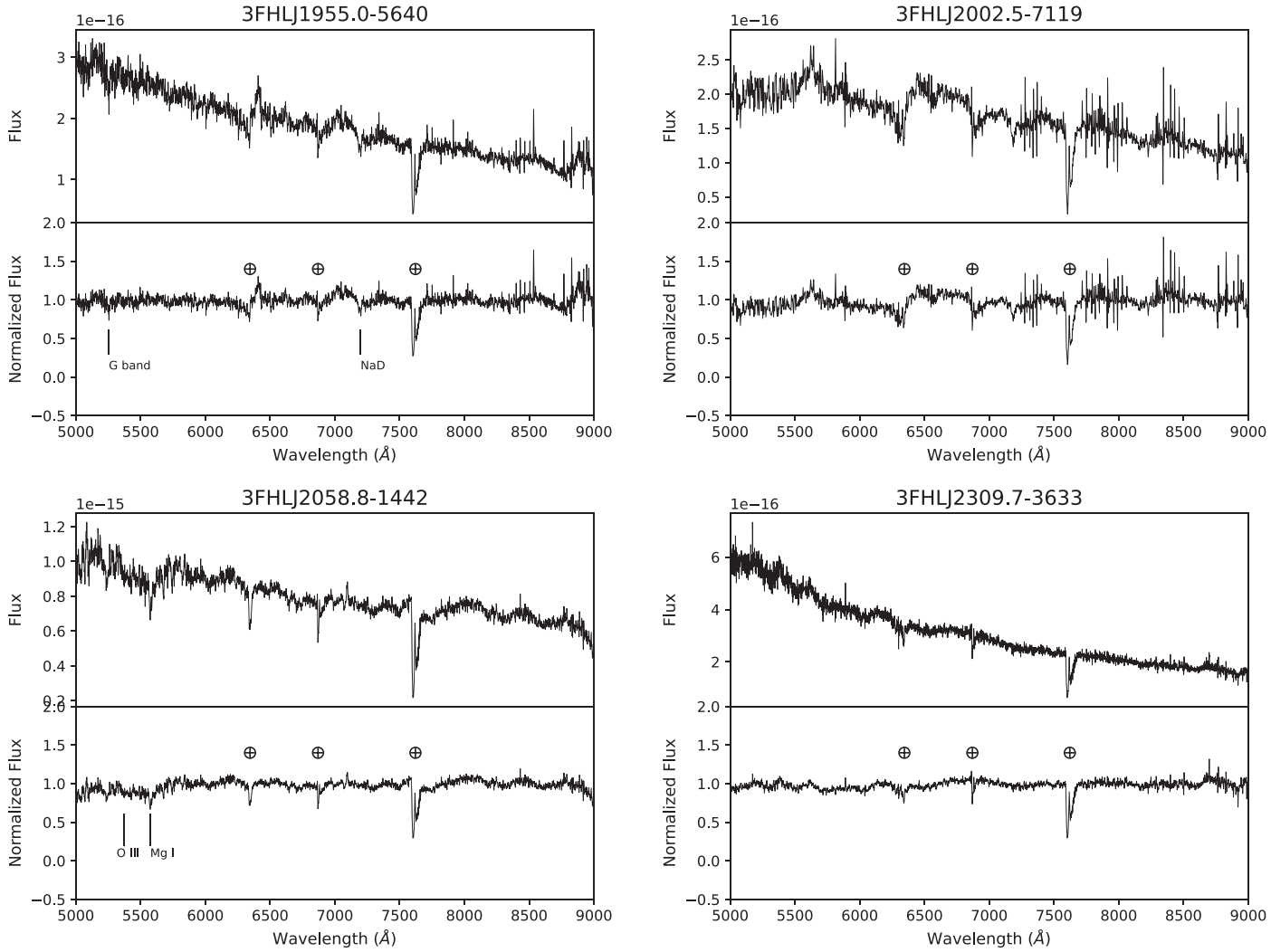

Figure 1. (Continued.)

13. *3FHL J1442.5−4621*. This source displays absorption lines at 5698 Å, 5806 Å, and 6492 Å, which are attributed to the Mg I, Ca+Fe, and NaD lines, respectively. An emission line at 5517 Å (O III, EW = 1.5 Å) was also observed. This leads to a redshift of $z = 0.102$, confirming the measurement by the 6dF Galaxy Survey (Jones et al. 2009). This source has been classified as a BL Lac in the 4FGL catalog. Our results are in agreement with this classification. This source has been reported as an HSP blazar in 4LAC.
14. *3FHL J1455.4−7559*. This source displayed a featureless optical spectrum and has been reported by the 4LAC to be an HSP blazar.
15. *3FHL J1457.8−4642*. In the optical spectrum, absorption lines were detected at 5744 Å and 5851 Å. These lines are attributed to Mg I and Ca+Fe lines, respectively. An emission line detected at 5372 Å (EW = 0.6 Å) could possibly be due to Hβ. These features give us a redshift measurement of $z = 0.10$. We classify this source as a BL Lac. This source has no reported SED class in the Fermi-LAT catalogs.
16. *3FHL J1514.7−0949*. This source displayed a featureless optical spectrum and has been classified by the 4LAC to be an LSP blazar.
17. *3FHL J1542.1−2915*. A particularly noisy spectrum was obtained for this source, due to which we were unable to identify any features. Thus, we tentatively classify this source as a BL Lac. This source is an HSP blazar in 4LAC.
18. *3FHL J1549.7−3045*. The optical spectrum of this source was featureless. This source is an HSP blazar in 4LAC.
19. *3FHL J1604.6−4441*. This source's optical spectrum was observed to be featureless. This object has been classified as an LSP blazar in 4LAC.
20. *3FHL J1647.3−6438*. The optical spectrum for this source exhibits an absorption doublet at 7195 and 7230 Å. These lines correspond to Ca II lines, yielding a lower limit of $z > 0.82$. We classify this source as a BL Lac. This source is classified as an LSP blazar in 4LAC.
21. *3FHL J1849.2−1647*. The optical spectrum for this source displayed three absorption features at 8537, 8659, and 8805 Å. If the first two features are attributed to Mg I and Ca+Fe, then we obtain $z > 0.64$. On the other hand, if the feature at 8659 Å is due to Mg I, then the feature at 8805 Å can be attributed to Ca+Fe, yielding $z > 0.67$. We classify this source as a BL Lac. This source is classified as an HSP blazar in 4LAC.

22. *3FHL J1934.2−2419*. This source displayed a featureless optical spectrum and has been reported by the 4LAC catalog to be an HSP blazar.
23. *3FHL J1944.4−4523*. In the optical spectrum for this source, three absorption features were detected. These three features are at 7274 Å (*G*-band), 8704 Å (Mg I), and 8916 Å (Ca+Fe), yielding $z > 0.68$. We classify this source as a BL Lac. This source has no reported SED class in the Fermi-LAT catalogs.
24. *3FHL J1944.9−2143*. In this optical spectrum, absorption features were detected at 7289 and 7435 Å. These correspond to Mg I and Ca+Fe lines, respectively, yielding a lower limit, $z > 0.41$. This result agrees with the value reported by Chang et al. (2017) in the 2WHSP catalog. This lower-limit value was obtained by the authors using the same technique as the 1WHSP catalog (described for the source 3FHL J0102.8–2001). We classify this source as a BL Lac. This source has no reported SED class in the Fermi-LAT catalogs.
25. *3FHL J1955.0−5640*. In the optical spectrum for this source, two absorption features were identified at 5255 Å (*G*-band) and 7198 Å (NaD). This gives us a lower limit of $z > 0.22$ for this source. We classify this source as a BL Lac. Our results are in mild disagreement with the redshift value reported by Marchesini et al. (2019) of $z = 0.22$. The authors also observed absorption features for this source that they attributed to the host galaxy instead. Their optical spectra for this source was obtained using the 4.1 m SOAR telescope, located in Chile. This source is an HSP blazar according to 4LAC.
26. *3FHL J2002.5−7119*. This source exhibited a featureless optical spectrum and has no reported SED class in the 4LAC.
27. *3FHL J2058.8−1442*. This source displayed an emission peak at 5375 Å that is due to O III (EW = 0.4 Å) and an absorption feature at 5574 Å, due to Mg I. This allows us to confirm the redshift of $z = 0.07$ for this source as reported by Jones et al. (2009). We classify this source as a BL Lac. This source has no reported SED class in the Fermi-LAT catalogs.
28. *3FHL J2309.7−3633*. This source exhibited a featureless optical spectrum and has been reported as an HSP blazar in the 4LAC.

5. Discussion and Conclusions

This identification campaign to classify BCUs in the 3FHL catalog and to measure their redshift began in 2017, when 36 unassociated sources (out of 52 chosen) from 3FHL catalog were classified as BL Lacs with the help of machine-learning algorithms (Kaur et al. 2019). For the second part of this campaign, 28 sources were observed with the 4 m telescope at the Kitt Peak National Observatory (KPNO) in Arizona, in order to perform optical spectroscopy. These results were published in Marchesi et al. (2018), where 27 sources were classified as BL Lacs and one as an FSRQ. Redshift measurements or lower limits were also provided for seven of these sources. The third part of the campaign, for which spectra for 23 sources were obtained using the 4 m telescope at CTIO in Chile, resulted in the categorization of all 23 sources as BL Lacs and the determination of redshift estimates or lower limits for eight sources (Desai et al. 2019). The fourth paper from this campaign resulted in the classification of 15 sources (out of 38) as BL Lacs using machine-learning algorithms (Silver et al. 2020).

There are other works that are complementary to our campaign toward completing the 3FHL catalog. For instance, Paiano et al. (2017, 2019, 2020) have studied 103 Fermi-LAT sources so far and provided redshifts for 65 of them. As part of a large spectroscopic program, Peña-Herazo et al. (2020) have classified 350 Fermi-LAT sources into BL Lac and FSRQ categories. Landoni et al. (2020) have compiled a database of spectroscopic redshifts of BL Lacs that is available online.[9]

We present here the results of the fifth part of this ongoing optical spectroscopic campaign aimed at the spectral completeness of the 3FHL catalog. We report on 28 sources observed with the COSMOS spectrograph mounted on the 4 m Blanco telescope, located at the CTIO facility in Chile. Based on the optical spectra of our sources, 25 sources were classified as BL Lacs, and the remaining three were classified as FSRQs.[10] With ∼85% of the sources in the 3FHL catalog being BL Lacs, these classification results are not unexpected. Desai et al. (2019) found all (23) sources observed by them to be BL Lacs, while Marchesi et al. (2018) identified 27 sources as BL Lacs, out of the 28 observed.

We were also able to place redshift constraints on 57% (16/28) of our sources representing a significant improvement in the success rate of such campaigns with 4 m class telescopes (see Landoni et al. 2015; Ricci et al. 2015; Álvarez Crespo et al. 2016a; Peña-Herazo et al. 2017).

The completeness plots for our campaign sources with respect to all blazars in the energy range of 10 GeV–2 TeV are shown in Figure 2. The latest release of the fourth catalog of AGN detected by the Fermi-LAT (4LAC–DR2; Ajello et al. 2020) was used to update the 3FHL catalog in order to include recent redshift measurements and classifications of sources as provided by various campaigns (e.g., Peña-Herazo et al. 2017, 2020; Paiano et al. 2019, 2020; de Menezes et al. 2020). Completeness was obtained by considering the ratio of the number of classified blazars or blazars with z above a given flux divided by the total number of blazars in the same range. As seen from this figure, this campaign has substantially increased the type completeness of the sources in 3FHL catalog, but less so the redshift completeness. Prior to our campaign, 21% of the 3FHL blazars lacked a type and 45% lacked a redshift value. With our campaign, we were able to decrease the fraction of blazars without a type to ∼12% and blazars without redshift to 43%. The type completeness also reaches 95% for $F > 3 \times 10^{-12}$ erg cm^{-2} s^{-1} (see Figure 2, left).

Hence, even with 4 m class telescopes like KPNO and CTIO, we have made significant progress in achieving our goal of full completeness in the 3FHL catalog. But since the success rate of redshift determination with 8 m class telescopes is even higher (60%–80%), for the next part of our campaign we will present the results of the observations undertaken using the 8 m Gemini-N and -S telescopes.

Identification of classes and redshifts of high-energy sources is also a crucial step in understanding and constraining the EBL (e.g., Saldana-Lopez et al. 2020). The cosmic gamma-ray horizon (CGRH) provides an estimate of the distance beyond

[9] https://web.oapd.inaf.it/zbllac/

[10] Two of these being tentative classifications (for 3FHL J0001.9−4155 and 3FHL J0102.8−2001).

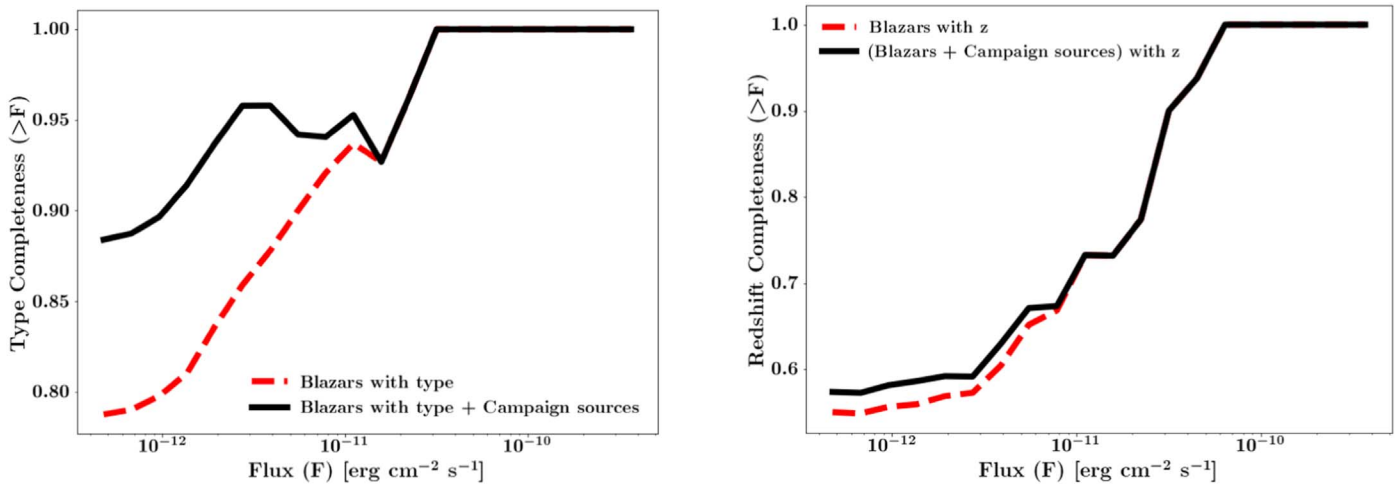

Figure 2. Completeness as a function of energy flux in the 3FHL energy range (10 GeV–2 TeV). At each flux, $f > F$, we take the total number of sources with type/redshift and divide it by the total number of sources. Left panel: The type completeness has been computed by considering the number of blazars with classification (or type) with respect to the total number of blazars (red dashed line). Including the contribution of this campaign to the number of classified blazars (solid black line) shows an increase in the overall completeness. Right panel: The redshift completeness for blazars with a measured z value with respect to the total number of blazars has been plotted by the dashed red line. After including the contribution of this campaign to the overall number of blazars with z (solid black line), there is an increase in the z completeness.

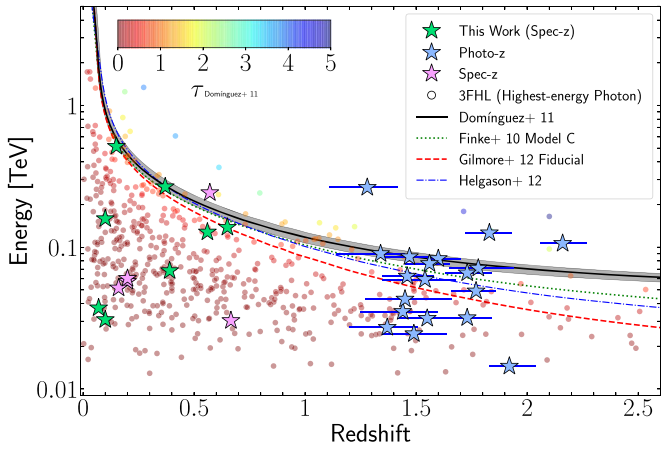

Figure 3. Estimation of the CGRH as a function of redshift. The data points and some of the models have been adapted from Figure 17 of Ajello et al. (2017). The HEP from 3FHL catalog are plotted as colored circles. The color of the circles represents the corresponding optical depth values as shown in the color bar. The predictions from different EBL models (Finke et al. (2010; dotted green line), Domínguez et al. (2011; solid black line, with uncertainties shown as the shaded band), Gilmore et al. (2012; dashed red line), and Helgason & Kashlinsky (2012; dotted–dashed blue line)) are shown for comparison. The pink and green stars report the HEP for sources from the spectroscopic campaign, while the blue stars represent the HEP for sources from the photometric campaign (Rau et al. 2012; Kaur et al. 2017, 2018; Rajagopal et al. 2020).

which the universe becomes opaque to gamma-rays ($\tau_{\gamma\gamma} = 1$, where $\tau_{\gamma\gamma}$ is the optical depth of EBL as estimated from the models). This opacity originates when very high-energy ($E > 100$ GeV) photons interact with the low-energy EBL photons causing electron–positron pair production to occur, thus annihilating the photons in the process (Domínguez et al. 2013). The CGRH as a function of redshift has been plotted in Figure 3 for all the highest-energy photons (HEP) in the 3FHL catalog (Ajello et al. 2017). We highlight in the figure both the objects studied in our spectroscopic campaign and the photometric campaign. The photometric dropout technique is based on the flux attenuation caused by the interaction of source photons by neutral hydrogen and it becomes particularly effective at $z > 1$ (Rau et al. 2012; Kaur et al. 2017, 2018; Rajagopal et al. 2020). It is clear that both campaigns resulted in several sources for which the HEPs are very near current estimates of the CGRH, as well as some beyond the horizon.[11] Thus, such campaigns are invaluable in further constraining the CGRH as well as probing higher-opacity regions, e.g., $\tau_{\gamma\gamma} \gtrsim 2$, where redshift data are sparse. Estimating a redshift for such high-energy sources will enable a better and more accurate measurement of the EBL.

M.R., S.M., and M.A. acknowledge support from NASA contract 80NSSC19K0151. A.D. is thankful for the support of the Ramón y Cajal program from the Spanish MINECO. The authors thank Alberto Alvarez, Claudio Aguilera, and Sean Points for the help provided during the observing nights at CTIO. This work made use of the TOPCAT software for the analysis of data tables.

ORCID iDs

M. Rajagopal https://orcid.org/0000-0002-8979-5254
A. Kaur https://orcid.org/0000-0002-0878-1193
A. Domínguez https://orcid.org/0000-0002-3433-4610
R. Silver https://orcid.org/0000-0001-6564-0517
M. Ajello https://orcid.org/0000-0002-6584-1703

References

Abdo, A. A., Ackermann, M., Ajello, M., et al. 2011, ApJ, 727, 129
Abdollahi, S., Acero, F., Ackermann, M., et al. 2020, ApJS, 247, 33
Abdollahi, S., Ackermann, M., Ajello, M., et al. 2018, Sci, 362, 1031
Abramowski, A., Acero, F., Aharonian, F., et al. 2012, A&A, 548, A38
Ackermann, M., Ajello, M., Allafort, A., et al. 2012, Sci, 338, 1190
Ajello, M., Angioni, R., Axelsson, M., et al. 2020, ApJ, 892, 105
Ajello, M., Atwood, W. B., Baldini, L., et al. 2017, ApJS, 232, 18
Ajello, M., Romani, R. W., Gasparrini, D., et al. 2014, ApJ, 780, 73
Álvarez Crespo, N., Masetti, N., Ricci, F., et al. 2016a, AJ, 151, 32

[11] The source from the spectroscopic campaign that lies beyond $\tau > 1$ is 1RXS J013427.2+263846, which has an HEP of 242 GeV and $z = 0.57$ (Marchesi et al. 2018).

Álvarez Crespo, N., Massaro, F., Milisavljevic, D., et al. 2016b, AJ, 151, 95
Arsioli, B., Fraga, B., Giommi, P., Padovani, P., & Marrese, P. M. 2015, A&A, 579, A34
Atwood, W. B., Abdo, A. A., Ackermann, M., et al. 2009, ApJ, 697, 1071
Bade, N., Beckmann, V., Douglas, N., et al. 1998, A&A, 334, 459
Chang, Y. L., Arsioli, B., Giommi, P., & Padovani, P. 2017, A&A, 598, A17
de Menezes, R., Amaya-Almazán, R. A., Marchesini, E. J., et al. 2020, Ap&SS, 365, 12
Desai, A., Helgason, K., Ajello, M., et al. 2019, ApJL, 874, L7
Desai, A., Marchesi, S., Rajagopal, M., & Ajello, M. 2019, ApJS, 241, 5
Domínguez, A., & Ajello, M. 2015, ApJL, 813, L34
Domínguez, A., Finke, J. D., Prada, F., et al. 2013, ApJ, 770, 77
Domínguez, A., Primack, J. R., Rosario, D. J., et al. 2011, MNRAS, 410, 2556
Domínguez, A., Wojtak, R., Finke, J., et al. 2019, ApJ, 885, 137
Finke, J. D., Razzaque, S., & Dermer, C. D. 2010, ApJ, 712, 238
Furniss, A., Williams, D. A., Danforth, C., et al. 2013, ApJL, 768, L31
Ghisellini, G., Righi, C., Costamante, L., & Tavecchio, F. 2017, MNRAS, 469, 255
Gilmore, R. C., Somerville, R. S., Primack, J. R., & Domínguez, A. 2012, MNRAS, 422, 3189
Helgason, K., & Kashlinsky, A. 2012, ApJL, 758, L13
Jones, D. H., Read, M. A., Saunders, W., et al. 2009, MNRAS, 399, 683
Kaur, A., Ajello, M., Marchesi, S., & Omodei, N. 2019, ApJ, 871, 94
Kaur, A., Rau, A., Ajello, M., et al. 2017, ApJ, 834, 41
Kaur, A., Rau, A., Ajello, M., et al. 2018, ApJ, 859, 80
Landoni, M., Falomo, R., Paiano, S., & Treves, A. 2020, ApJS, 250, 37
Landoni, M., Massaro, F., Paggi, A., et al. 2015, AJ, 149, 163
Malkin, Z. M. 2016, ARep, 60, 996
Maraschi, L., Ghisellini, G., & Celotti, A. 1994, in IAU Symp. 159, Multi-wavelength Continuum Emission of AGN (Dordrecht: Kluwer Academic), 221
Marcha, M. J. M., Browne, I. W. A., Impey, C. D., & Smith, P. S. 1996, MNRAS, 281, 425
Marchesi, S., Kaur, A., & Ajello, M. 2018, AJ, 156, 212
Marchesini, E. J., Peña-Herazo, H. A., Álvarez Crespo, N., et al. 2019, Ap&SS, 364, 5
Massaro, E., Giommi, P., Leto, C., et al. 2009, A&A, 495, 691
Massaro, F., Masetti, N., D'Abrusco, R., Paggi, A., & Funk, S. 2014, AJ, 148, 66
Paggi, A., Milisavljevic, D., Masetti, N., et al. 2014, AJ, 147, 112
Paiano, S., Falomo, R., Franceschini, A., Treves, A., & Scarpa, R. 2017, ApJ, 851, 135
Paiano, S., Falomo, R., Treves, A., Franceschini, A., & Scarpa, R. 2019, ApJ, 871, 162
Paiano, S., Falomo, R., Treves, A., & Scarpa, R. 2020, MNRAS, 497, 94
Paliya, V. S., Domínguez, A., Cabello, C., et al. 2020, ApJL, 903, L8
Peña-Herazo, H. A., Amaya-Almazán, R. A., Massaro, F., et al. 2020, A&A, 643, A103
Peña-Herazo, H. A., Marchesini, E. J., Álvarez Crespo, N., et al. 2017, Ap&SS, 362, 228
Rajagopal, M., Kaur, A., Ajello, M., et al. 2020, ApJ, 898, 18
Rau, A., Schady, P., Greiner, J., et al. 2012, A&A, 538, A26
Ricci, F., Massaro, F., Landoni, M., et al. 2015, AJ, 149, 160
Saldana-Lopez, A., Domínguez, A., Pérez-González, P. G., et al. 2020, arXiv:2012.03035
Sbarufatti, B., Treves, A., Falomo, R., et al. 2005, AJ, 129, 559
Schlafly, E. F., & Finkbeiner, D. P. 2011, ApJ, 737, 103
Shaw, M. S., Romani, R. W., Cotter, G., et al. 2012, ApJ, 748, 49
Shaw, M. S., Romani, R. W., Cotter, G., et al. 2013, ApJ, 764, 135
Silver, R., Marchesi, S., Marcotulli, L., et al. 2020, ApJ, 902, 23
Stickel, M., Padovani, P., Urry, C., Fried, J., & Kuehr, H. 1991, ApJ, 374, 431
Tody, D. 1986, Proc. SPIE, 627, 733
Truebenbach, A. E., & Darling, J. 2017, ApJS, 233, 3
Urry, C. M., & Padovani, P. 1995, PASP, 107, 803
van den Berg, J. P., Böttcher, M., Domínguez, A., & López-Moya, M. 2019, ApJ, 874, 47